Polytypism in decagonal quasi-crystals and approximant crystals

1992 J. Phys.: Condens. Matter 4 10169

(http://iopscience.iop.org/0953-8984/4/50/008)

J. Phys.: Condens. Matter 4 (1992) 10169–10198. Printed in the UK

Polytypism in decagonal quasi-crystals and approximant crystals

Song-Seng Kang and Jean-Marie Dubois

Laboratoire de Science et Génie des Matériaux Métalliques, CNRS UA159, Ecole des Mines, Parc de Saurupt, F-54042 Nancy, France

Received 10 July 1992, in final form 25 September 1992

Abstract. A classification scheme, which is able to relate many crystalline compounds to the decagonal quasi-crystalline phases, is given based on a description of the atomic decoration in terms of a small number of subtiling units. This scheme is suitable for one-dimensional sequences, two-dimensional tilings and three-dimensional networks. The relative numbers of each type of tiling unit in the Penrose pattern are calculated. The paper first focuses on the two-dimensional aperiodic plane. In a way reminiscent of polytypism, a distinction is then made according to the way such planes are stacked periodically on top of each other, thus giving insight into the structure of the known decagonal phases. Emphasis is then put on the aperiodic scheme, which may be related to non-ideally ordered icosahedral phases. This way of describing the structure allows us to construct atomic models in three dimensions and to calculate accordingly the composition of the model structure starting from a known crystalline phase with identical or closely related composition. Many approximant and quasi-crystalline structures, not all yet observed experimentally, may be sorted out.

1. Introduction

Quasi-crystalline phases are most often associated with crystalline compounds, either because they form simultaneously within the same specimen or because their compositions are closely related. Such crystals are usually characterized by large unit cells and show in reciprocal space scattering patterns that are reminiscent of those of the true quasi-crystals [1]. The structures of these crystalline compounds, the so-called approximants, are constructed with subtiling units (for example, the convex pentagon) identical to those observable by high-resolution electron microscopy (HREM) in the quasi-crystalline phases when looked at along a forbidden crystallographic axis (i.e. fivefold, 10-fold, pseudo-10-fold [2–4]. Altogether, the quasi-crystalline and approximant phases contribute in a very fascinating way to what is called polymorphism. Since there are more and more new approximants discovered in quasi-crystal-forming alloys, we propose here (section 2) a classification scheme that will enable us to relate many approximant structures to each other as well as to the quasi-crystalline phases in a simple way. Two types of quasi-crystalline phases are considered. The decagonal phase [5] on the one hand is a periodic packing along a 10-fold axis of aperiodic atomic planes. On the other hand, aperiodic stacking of aperiodic planes along a common fivefold axis produces a quasi-periodic network, which, despite not exhibiting the perfect $m\bar{3}\bar{5}$ point group symmetry assigned to the

0953-8984/92/5010169+30$07.50

icosahedral phase [6], is worth considering. Although entropy stabilization may play a great role, both structures in two-dimensional (2D) real space may be preferably represented by a Penrose tiling (PT) [7] pattern when viewed along a forbidden crystallographic axis.

The structural details of a 2D quasi-crystal were sorted out by Steurer and Kuo [8] for the decagonal d-Al–Cu–Co(Si) [9] system. Before this experimental result, Kumar *et al* [10] had proposed some candidate decoration models of the decagonal phase based on crystalline Al_6Mn [11] and $Al_{13}Fe_4$ [12] structures. They proposed to rely upon two types of layers for the construction of the decagonal phase. However, models in three dimensions incorporating the periodic stacking sequence cannot be constructed owing to the different periodicities found in the crystalline phase (8.1 Å for $Al_{13}Fe_4$ [12]) on the one hand and the decagonal phase (16.5 Å for Al-Fe [13,14]) on the other. Thus, no calculation of the composition of the simulated decagonal structure can be made. It is the aim of the present paper to propose a method that is able to calculate the composition of a highly ordered quasicrystalline phase. At the same time, a three-dimensional structure can be specified in detail.

The ideal icosahedral structure is often attributed to a 3D PT model [15,16]. It is packed by only two tiling units: prolate rhombohedron and oblate rhombohedron. It has been used to a large extent, especially for structure simulation and indexation problems of icosahedral phases [17–24]. Quite generally however, the Penrose rhombohedra have different internal atomic configurations [22–29]. Different models have been proposed to decorate this 3D PT model by placing atoms within the rigid geometry [22–25]. Guyot and Audier [22] based a model on local atomic configurations similar to the crystalline Al–Mn–Si α-phase [17]. An analysis of the α-phase in terms of rhombohedra similar to the tiling units of the 3D PT packing was carried out by Henley and Elser [23]. Another structure model has been derived by Janot *et al* [25] from a 6D crystallographic analysis of neutron scattering data, beyond the determination of partial pair distribution functions [30] in the i-Al–Mn icosahedral phase.

Duneau and Oguey [21] have also proposed a model for the icosahedral i-Al–Mn–Si quasi-crystal built by a cut method. Their model uses the 3D PT as a reference frame to fix the atom positions and to describe local patterns as proposed in [18,23,27,31,32]. Two types of clusters, dodecahedral and rhombic triacontahedral, enter in the construction of polyhedral atomic surfaces. Successive refinements are related to replacing a small dodecahedron by a small rhombic triacontahedron and further on by a larger dodecahedron and a rhombic triacontahedron. The way polyhedra are generated is quite similar to our structure description used here. Instead of using the 3D PT, we ground our model on an algorithm consisting of stacking 2D PT networks, which will by the way generate different polyhedra from small size to larger size. We will see later that the calculated stoichiometry comes very close to the composition estimated experimentally for the icosahedral i-Al–Mn phase without silicon.

This paper consists of two main parts. The first one focuses on the classification scheme. This scheme is based, on the one hand, on a small number of tiling units that construct the periodic or quasi-periodic planes; and, on the other hand, on the stacking sequences of these periodic or quasi-periodic planes along the perpendicular direction. It is suitable for one-dimensional (1D), two-dimensional (2D) and three-dimensional (3D) classifications. The 1D scheme is characterized by two segments, one long (L) and one short (S), and is given basically for the sake of illustration. The 2D

scheme is characterized by tiling units such as the convex pentagon, the thin rhombus, etc. The 3D scheme works out stacking sequences of the previous 2D tilings (and not 3D tiling units as is usually considered in the literature). Periodic sequences are relevant to the decagonal phase (and relative approximant crystals). Meanwhile, the perfect icosahedral phase necessarily requires that the atomic number density varies continuously from one plane to the next one and therefore cannot be constructed by a finite set of planes or sheets. If the number of sheets is finite, the resulting network may nevertheless be truly aperiodic in 3D provided both the planes and the stacking along the perpendicular direction obey a quasi-periodic construction scheme. This specific case will be examined to some extent in the following although the network will no longer strictly exhibit the $m\bar{3}\bar{5}$ point group symmetry.

The purpose of this part of the paper is to focus attention onto atomic sheets, planar as well as corrugated, observable in known approximant phases. Equivalent sheets adapted to the quasi-crystalline structures may be deciphered from the previous ones by applying suitable symmetry operations. Then, stacking these sheets on top of each other along a fivefold axis produces a 3D model within the limits of stereological constraints that are specified. This way of looking at quasi-crystals and related crystals is very close to the method adopted for polytypes. The main difference with the field of polytypes is that, instead of honeycomb or triangular lattice planes, we will stack Penrose 2D-lattice planes, either truly aperiodic, suitable for quasi-crystals, or approximant, which are needed to build the crystal structures. Penrose lattice planes are used herein because they are unequivocally defined, despite the fact that we realize that random-tiling planes are presumably better adapted to quasi-crystals; see discussion in [33]. These 2D lattice planes or layers carry the appropriate atomic species. This will lead to a satisfactory understanding of the relevant structural conditions for a specific quasi-periodic structure to form.

Elaborating on the previous results, the second main part of the paper is a report on evaluating the composition of a decagonal phase in an alloy system knowing an approximant structure. We first calculate the relative number of each tiling unit constructing the 2D lattice (e.g. the Penrose tiling pattern). The second stage consists of decorating 2D units similar to the ones in the crystalline phase. Depending on how the 2D lattices are stacked, the composition can then be calculated according to the number of 2D lattices building the 3D structure model. Two specific quasi-crystalline phases, namely the decagonal d-Al–Mn–(Ni) and the icosahedral i-Al–Mn–(Ni) phases, are studied, from the points of view of both model building and experimental studies of real samples by diffraction techniques. Thus, the paper will provide clues to understanding how structural units, which entail the fivefold orientational order, match together to form either the approximant crystals or the quasi-crystalline phases.

2. Classification scheme

2.1. One-dimensional classification

The Fibonacci sequence is a quasi-periodic succession of two intervals, one long (L) and another short (S), having for instance a length ratio equal to τ. It can be generated by an iterative procedure of transformation in either deflation or inflation modes. In the τ^{-1} deflation construction, one long segment L transforms to the sequence $L^{-}S^{-}$ and one short segment S transforms to a long segment L^{-} (and

vice versa for a τ inflation construction). If the length ratio is taken as $L/S = \tau$, then unambiguously, one may identify $S = 1$, $L = \tau$, $S^- = 1/L = \tau^{-1}$, $L^- = 1$, $S^+ = \tau$, $L^+ = 1 + L = \tau^2$ in arbitrary length units. This procedure embodies the self-similar properties of the structure. Among the methods used to construct the self-similar sequences, the strip method is one of the most frequently employed in such a description [18,34,35]. A strip cut through a 2D square lattice having irrational slope i.e. $m = \tau$, gives a 1D analogue of the Penrose tiling. Alternatively, a strip tilted to have slope m rational gives a periodic tiling. In this periodic tiling, each unit cell is constructed by both segments L and S. It is actually a fragment of the Fibonacci quasi-periodic sequence that contains the origin. It fits better and better to the quasi-periodic tiling with increasing length of the unit cell. Since all sequences that form according to the value of m, either rational or irrational, contain the two units L and S, we may label them according to the number of units they contain, i.e. $\tau^{\pm 1,0}(N_i)$, where exponent $+1$ labels an inflation mode, -1 a deflation mode, 0 the normal sequence and $N_i (i = \text{L or S})$ is the number of segments L and S. The length of the 1D unit cell repeated periodically along the sequence is given by $\tau^n d_0$, where n is the order number of the sequence (see table 1) and d_0 is the length of the long segment L. Table 1 presents a list of tiling notations for a few approximant 1D sequences. The ratio N_L/N_S in the rational sequence corresponds to the slope m. In the quasi-crystalline case, this ratio is taken equal to τ.

2.2. Two-dimensional classification

Two such 1D sequences, oriented along two directions separated by an angle of $2\pi/10$, may be used to generate a 2D tiling. The generation of these 2D packings is equivalent to the projection on the 2D plane of a 2D strip lifted in a 4D periodic lattice. Two examples of approximant tilings generated by two 1D sequences with $m_1 = 3/2$ and $m_2 = 5/3$ are shown in figure 1. The Bravais lattice of these approximant networks is face-centred orthorhombic. In this figure, two sets of possible tiling elements are used to tile the lattice. The first set consists of the (fat) f-rhombus and the (thin) t-rhombus, while the second set consists of the (convex) v-pentagon, the (concave) c-pentagon and the (thin) t-rhombus (figure 2). These two sets of tiling elements share common points. For an identical unit length d_0 of segment L in the 1D tiling, two t-rhombuses and one f-rhombus form a hexagonal cell, which can be equally well filled with one c-pentagon and one v-pentagon. Also one v-pentagon can decompose into one f-rhombus and one c-pentagon.

As in the 1D classification case, the 2D scheme of the periodic (approximant) and quasi-periodic (Penrose tiling) patterns are classified according to the numbers of tiling elements constructing the unit cell. Instead of two segments L and S, the 2D tiling elements are the f, t, v or c units. A notation based on the segments L and S of the m_1 and m_2 sequences would not define the tiling unequivocally any more, whereas the 2D tiling units do. We define a general notation as $\tau^n(N_i \ldots)$, where N_i is the number of element of type i = f, t, v, c and n is the position of the tiling in the inflation (n has positive sign) or deflation (n has negative sign) sequence. For the Penrose pattern, the packing notation is $\tau^n(\infty_f \infty_t)$ or $\tau^n(\infty_v \infty_t \infty_c)$ depending on which set of tiling elements is employed. Table 2 presents some examples of the notation for the planes perpendicular to the fivefold axis or pseudo-fivefold axis in the quasi-crystalline cases and the approximant cases, respectively. Indeed, most of the 2D patterns of the approximant phases can be referred to a family group. For instance, let us consider only the constitutive units of the patterns. Then, the tiling patterns of

Table 1 One dimensional classification.

order number n	slope m	τ^{+1} inflation sequence	number of tiles	notation	length of cell	τ^{0} normal sequence	number of tiles	notation	length of cell	τ^{-1} deflation sequence	number of tiles	notation	length of cell
0	1/0	--	0	-	-	L	1	(1L)	(d_0)	L^-S^-	2	τ^{-1}(1L1s)	$\tau(\tau^{-1}d_0)$
1	1/1	L^+	1	τ(1L)	(τd_0)	LS	2	(1L1s)	$\tau(d_0)$	$L^-S^-L^-$	3	τ^{-1}(2L1s)	$\tau^2(\tau^{-1}d_0)$
2	2/1	L^+S^+	2	τ(1L1s)	$\tau(\tau d_0)$	LSL	3	(2L1s)	$\tau^2(d_0)$	$L^-S^-L^-L^-S^-$	5	τ^{-1}(3L2s)	$\tau^3(\tau^{-1}d_0)$
3	3/2	$L^+S^+L^+$	3	τ(2L1s)	$\tau^2(\tau d_0)$	LSLLS	5	(3L2s)	$\tau^3(d_0)$	$L^-S^-L^-L^-S^-L^-S^-L^-$	8	τ^{-1}(5L3s)	$\tau^4(\tau^{-1}d_0)$
4	5/3	$L^+S^+L^+L^+S^+$	5	τ(3L2s)	$\tau^3(\tau d_0)$	LSLLSLS	8	(5L3s)	$\tau^4(d_0)$	$L^-S^-L^-L^-S^-L^-S^-L^-$ $L^-S^-L^-L^-S^-$	13	τ^{-1}(8L5s)	$\tau^5(\tau^{-1}d_0)$
∞	τ-quasi-crystals	$L^+S^+L^+L^+S^+L^+$..	∞	τ(∞L∞S)	$\tau^{\infty}(\tau d_0)$	LSLLSLS..	∞	(∞L∞S)	$\tau^{\infty}(d_0)$	$L^-S^-L^-L^-S^-L^-$..	∞	τ^{-1}(∞L∞S)	$\tau^{\infty}(\tau^{-1}d_0)$

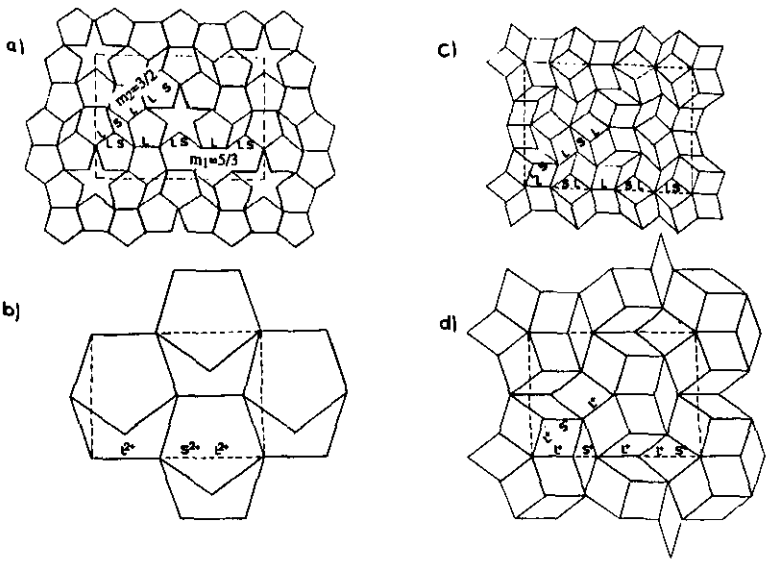

Figure 1. Four examples of 2D patterns with same unit cell illustrating $m_1 = 3/2$ versus $m_2 = 5/3$ approximants. A unit cell (broken lines) together with the 1D corresponding sequences are given in each pattern. (*a*) $(16_v6_t4_c)$ pattern, (*b*) $\tau^2(2_v2_c)$ pattern, (*c*) (26_f16_t) pattern and (*d*) $\tau(10_f6_t)$ pattern.

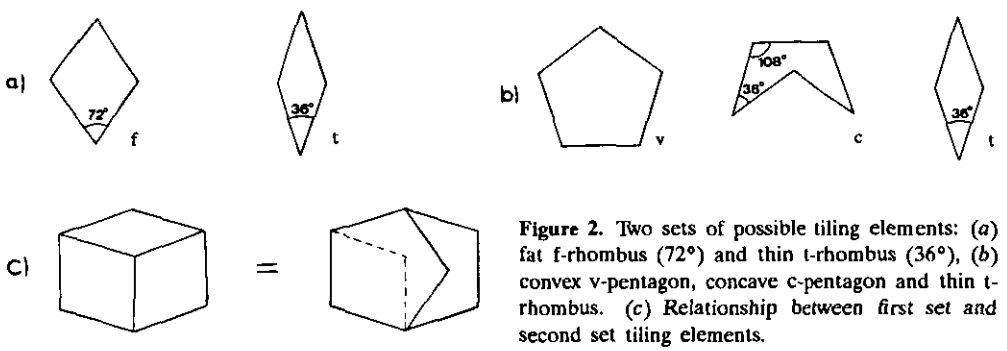

Figure 2. Two sets of possible tiling elements: (*a*) fat f-rhombus (72°) and thin t-rhombus (36°), (*b*) convex v-pentagon, concave c-pentagon and thin t-rhombus. (*c*) Relationship between first set and second set tiling elements.

the [0 1 0] projections of λ-$Al_{13}Fe_4$ [12] and ϕ1-$Al_{60}Mn_{11}Ni_4$ [36] phases are the same, four v-pentagons and two t-rhombuses constructing the structures. The compatible patterns, which are τ^2 and τ^3 times larger than the previous one, have been observed in the orthorhombic phases O_2 and O_2' forming the microcrystalline states in the Al–Cu–Fe–Cr (see figure 3) and Al–Cu–Co alloy systems [4], respectively. Another example can be seen in the [0 0 1] projection of β-Al_6Mn [11] (figure 4) and the [0 1 0] projection of the O_1 phase (orthorhombic structure that coexists with the O_2 phase forming the microcrystalline state in the Al–Cu–Fe–Cr alloys [4]).The pattern of the O_1 phase is τ^2 times larger in area than the one of β-Al_6Mn, two convex pentagons and two concave pentagons constructing the structures.

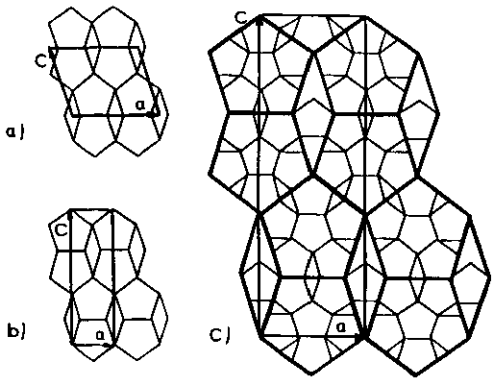

Figure 3. Three examples of the (2_v2_p)-type approximants: (*a*) λ-$Al_{13}Fe_4$, (*b*) ϕ1-$Al_{60}Mn_{11}Ni_4$ and (*c*) O_2-Al–Cu–Fe–Cr phase. The networks in (*a*) and (*b*) are drawn from crystallographic data reported in [12] and [36], respectively, whereas the network in (*c*) is conjectured from relevant HREM images.

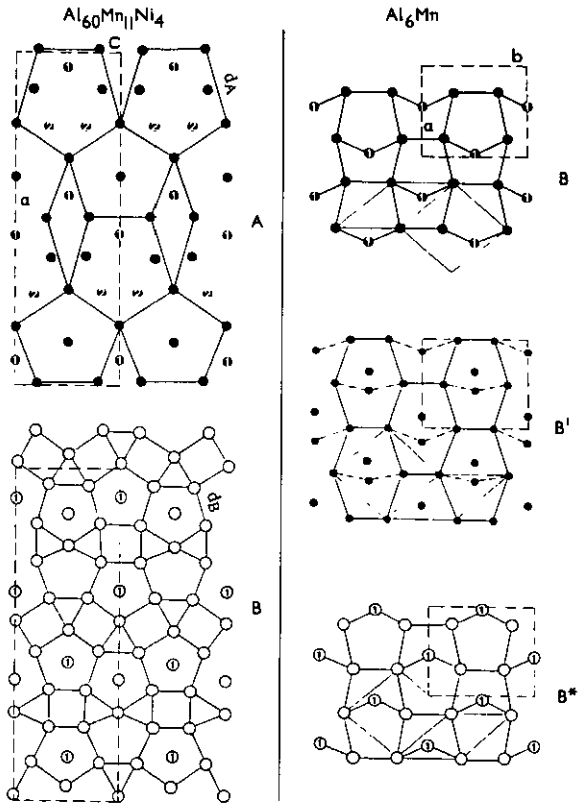

Figure 4. Crystal structures of orthorhombic β-Al_6Mn phase and orthorhombic ϕ1-$Al_{60}Mn_{11}Ni_4$ phase. The atoms marked with 1 and 2 are Mn and Ni, respectively. Open and full circles are Al.

2.3. Three-dimensional classification

Before attempting a classification in three dimensions, we introduce two examples of the approximant crystal structures; the orthorhombic β-Al_6Mn [11] and the orthorhombic ϕ1 phase [36], selected from among the approximant crystalline phases reported so far. Along the pseudo-fivefold axis, the structures are constructed by

stacking different types of atomic layers, which may be related to either one of two main types, A or B (see figure 4). These two types of layers were defined by their average sublattice edge length corresponding to $d_A \simeq 4.55$ Å and $d_B \simeq 2.8$ Å, respectively. The β-Al_6Mn orthorhombic phase consists of four layers stacked according to the sequence B′BB′B*: B and B* have identical atomic content and are related by the space group symmetry operations; B′ is different and contains only Al atoms. Conversely, the orthorhombic $\phi 1$ phase consists of six layers. Its sequence is BABB*A*B*. As above, the A* and B* sheets are variants of the A-type and B-type layers, respectively, obtained by applying the space group $Bbmm$ of the $\phi 1$ phase. In λ-$Al_{13}Fe_4$, a similar sequence may be defined, namely AB″A*B″. It contains four layers, two of the type already introduced above (A, A*) and two layers denoted B″, similar to the layer B in the $\phi 1$ phase but for a rotation of 36° around the 10-fold axis. We will see in the following section that this layer B″ can only lie next to a layer of type A. Both B′ and B″ layers correspond to B′* and B″* layers by space group symmetry. Such layers are shown explicitly in table 3 but we shall drop the asterisk in the following in order to simplify the notation, the space group shift of the B′ and B″ sheets being obvious from the notation carried by the adjacent A and B layers. The position of Al atoms in B-type layers is the same in both λ and $\phi 1$ phases, except for 36° rotation.

Table 2. Two-dimensional classification.

m_1 - m_2	Examples		Packing notations $\perp A_{10}$ (or pseudo A_{10})	
	cell parameters	corresponding axes	fat-f and thin-t rhombuses	convex-v pentagon, thin-t rhombus and concave-c pentagon
1/1 - 2/1	β-Al_6Mn a = 6.5 Å b = 7.55 Å c = 8.87 Å	1/1 -> [110] 2/1 -> [100]	(2_f)	$\tau^{-1}(2_v2_c)$
1/1 - 2/1	λ-$Al_{13}Fe_4$ a = 15.49 Å b = 8.08 Å c = 12.48 Å β = 107°43′ ϕ1-$Al_{60}Mn_{11}Ni_4$ a = 23.8 Å b = 12.5 Å c = 7.55 Å	1/1 -> [001] 2/1 -> [100] for λ-$Al_{13}Fe_4$ 1/1 -> [100] 2/1 -> [101] for ϕ1 phase	(6_f4_t) or $\tau(2_f2_t)$	(4_v2_t) or $\tau(1_v1_t1_c)$
3/2 - 5/3	O_1 a = 23.66 Å b = 12.27 Å c = 32.52 Å	3/2 -> [110] 5/3 -> [100]	(26_f16_t) or $\tau(10_f6_t)$ or $\tau^2(4_f2_t)$ or $\tau^3(2_f)$	$(16_v6_t4_c)$ or $\tau(6_v2_t2_c)$ or $\tau^2(2_v2_c)$
3/2 - 5/3	O_2 a = 20.10 Å b = 12.27 Å c = 61.94 Å	3/2 -> [110] 5/3 -> [110]	(36_f20_t) or $\tau^2(6_f2_t)$	$(26_v10_t6_c)$ or $\tau^2(4_v10_t)$
τ - τ	1) Al-Cu-Fe icosahedral phase a_6 = 6.5 Å† 2) Al-Cu-Co decagonal phase a_5 = 3.37 Å† c_5 = 4.15 Å†	τ -> 2-fold axis	$\tau^{\pm n}(\infty_f\infty_t)$	$\tau^{\pm n}(\infty_v\infty_t\infty_c)$

† parameter in high dimensional space.

Table 3. Three-dimensional classification.

Examples	d_3 (Å)	Stacking sequences	No. of layers D_3	Notation
β-Al_6Mn	8.87	B'BB'*B*	4	$4\,\tau^{-1}(2_v2_c)$
λ-$Al_{13}Fe_4$	8.083	AB"A*B"*	4	$4\,(4_v2_t)$
ϕ1-$Al_{60}Mn_{11}Ni_4$	12.5	ABB*A*B*B	6	$6\,(4_v2_t)$
O_1-AlCuFeCr	12.27	ABB*A*B*B	6	$6\,\tau^2(2_v2_c)$[a] or $6\,\tau^2\,(16_v6_t4_c)$[b]
O_2-AlCuFeCr	12.27	ABB*A*B*B	6	$6\,\tau^2(4_v2_t)$[a]
d-Al-Mn	12.4	B'BB*B'*B*B	6	D 6II[e]
d-Al-Mn-Ni	12.5	ABB*A*B*B	6	D 6II[e]
d-Al-Cu--Co	4.15	BB*	2	D 2II[e]
i-Al-Cu-Fe	∞	Aperiodic sequence	∞	see below
Icosahedron	8.636[c] 5.345[d]	see table 5	4 2	I 4II[e]
Dodecahedron	10.111[c] 6.259[d]		5 3	I 5II[e]
Icosadodecahedron	12.498[c] 7.742[d]		6 3	I 6II[e]
Rhombic triacontahedron	14.887[c] 9.379[d]		7	I 7II[e]

a - as revealed from HREM micrograph [34]. b - notation obtained from theoritical assumption.
c - values calculated from $d_A = 4.55$ Å = edge length in layer A.
d - values calculated from $d_B = 2.81$ Å = edge length in layer B.
e - notations: D = decagonal phase, I = icosahedral phase and II = $(\infty_v\infty_t\infty_c)$.

The average distance between two layers in the crystalline phases is about 2 Å. This value can be related to the periodic translation distance d_3 in all the decagonal phases found so far. For example, the decagonal phases of the Al–Mn, Al–Fe and Al–Cu–Co(Si) systems are constructed by a layering system along the 10-fold axis with six ($d_3 = 12.4$ Å), eight ($d_3 = 16.5$ Å) and two ($d_3 = 4.14$ Å) layers, respectively.

Thus, the 2D classification can be extended to a 3D scheme with only the addition of a third integer, namely the number D_3 of layers, in the perpendicular sequence (parallel to the 10-fold direction), that is $D_3\tau^n(N_i \ldots)$. This notation can be applied to all the approximant and quasi-crystalline phases, including the icosahedral phase, examined in the present paper as suggested in table 3. For icosahedral quasi-crystals, the number D_3 is infinite. The corresponding notation becomes $I\tau^n(\infty_f\infty_t)$ or $I\tau^n(\infty_v\infty_t\infty_c)$ where I stands for $D_3 = \infty$. We will see later in section 3.3 that various stacking algorithms adapted to the icosahedral phase may be distinguished within this scheme.

This 3D classification points out the distinction between two phases, for instance d-Al–Mn versus d-Al–Cu–Co and λ-$Al_{13}Fe_4$ versus ϕ1 phase, which eventually could not be distinguished according to the 2D scheme. For example, the 2D notation for both λ-$Al_{13}Fe_4$ and ϕ1 phase is (4_v2_p). Without considering the detail of the atomic decoration, these phases belong to the same class. As a matter of fact, their stacking

sequences in the third dimension are quite different. The sequence for λ-$Al_{13}Fe_4$ is AB″A*B″ (four layers) whereas it is ABB*A*B*B (six layers) for the ϕ1 phase.

3. Periodic versus aperiodic stacking sequences

Most of the approximant and decagonal structures are constructed by stacking one or two types of layers along the pseudo-10 and 10-fold axes, respectively, with periodicity corresponding to an even number of layers. Examples are the approximant ϕ1-$Al_{60}Mn_{11}Ni_4$ (six layers), decagonal d-Al–Fe (eight-layers) and d-Al–Cu–Co (two layers) phases. Why the decagonal and its approximant phases always consist of an even number of layers is not yet clear. Our first intention is to demonstrate that this is necessarily the case. The argument will be based on stacking layers of the type introduced in the previous section, yet satisfying topological constraints on the nature of the layer (A, A*, B, B*, B″) that may follow a sheet of a given type. Such constraints simply arise from tendency to close packing of metals and alloys and are readily observed in known approximant crystals.

A second point of interest is to know whether genuinely aperiodic 3D crystals may be accounted for as well by an appropriate sequence of atomic sheets. The (positive) answer to this question will also be elaborated in this section. As a result, a series of clusters with icosahedral point group symmetry (from icosahedron to rhombic triacontahedron) will be constructed according to distinct stacking sequences. Thirdly, we will shed some light on the difference between decagonal 2D and 3D aperiodic structures.

3.1. Flat and puckered atomic layers with fivefold symmetry

We have introduced in section 2.3 that the approximant crystal structures consist of atomic layers that may all be referred to two main types denoted A and B, respectively. There exist other layers, for instance A* and B*, which relate to the previous ones through symmetry operations of the space group. Sheets like A and A* (respectively B and B*) carry naturally the same atomic content. As already mentioned, it may be necessary to use other sheets to account appropriately for a given structure. The β-Al_6Mn compound requires also a layer B′ and the ϕ1 phase a complementary layer noted B″ in the previous section. This way of decomposing the structure into 2D elementary bricks has already been performed by several authors, see e.g. [8].

The atomic decoration characteristic of each approximant phase may be attached to the tiling units, for instance the convex pentagon and thin rhombus of the ϕ1 phase. There may be several possibilities to do so, but when a choice is made, the relationship between atomic decoration and tiling pattern is unequivocally defined. Yet, using a set of tiling units (i.e. t, v, c or t, f), a pattern with perfect fivefold symmetry around the origin may be constructed and furthermore decorated by the atoms attached to the units. A detailed example will be examined in section 5 to show how to solve the decoration of any unit, including the one which is not present in the approximant pattern (e.g. the v unit in the ϕ1 phase). Figure 5 presents the A-type and B-type sheets, having fivefold symmetry around an origin, that are produced from the corresponding sheets shown in figure 4, which have only broken fivefold symmetry. Using the classification scheme developed in section 2.2, it is straightforward to see that this peculiar choice of perfect fivefold symmetry is not the only possible one. Approximant 2D tilings of higher order than the ones illustrated in figure 4 may be

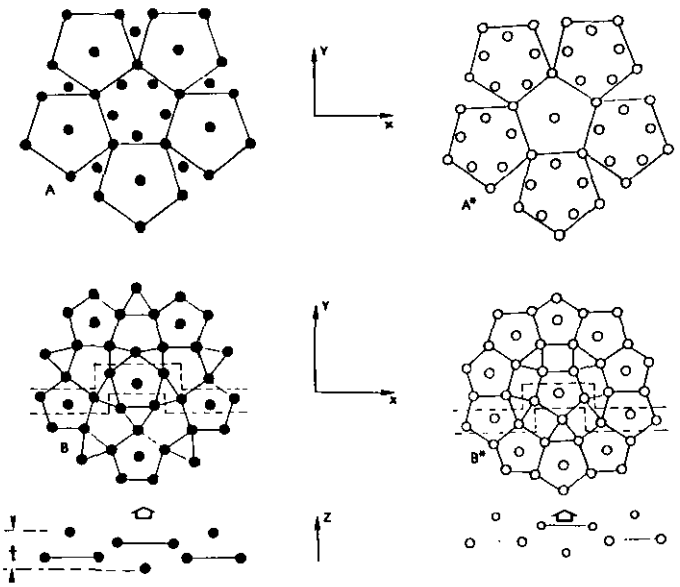

Figure 5. Examples of simulated aperiodic patterns, with a fivefold centre of symmetry, based on ϕ1-$Al_{60}Mn_{11}Ni_4$ subtiling elements and their atomic configurations. A and B are normal layers and A* and B* are two layers derived from the previous ones by applying respectively the symmetry operations of the space group. Below B and B* are shown two side views corresponding to the bands (broken lines) drawn in the layers B and B* to emphasize the corrugation of the layers in the space perpendicular to their plane.

constructed as well. In the following, we will, however, restrict ourselves to stacking layers with perfect fivefold symmetry.

An important point to raise at this stage is that all A-type layers are flat atomic planes whereas all B-type layers (B, B′, B″) are corrugated. They exhibit a thickness t from upper to lower atoms that is typically of the order of 1.5 Å (see the schematics laid out in the bottom part of figure 5, which presents a cut through the area of layers B, B* defined by broken lines). The edge length of each type of sheet is different, having $d_A = \tau d_B$ when the fivefold symmetry is perfect. The A-type patterns therefore map onto the B-type ones by a first-order inflation. These two differences, planarity versus corrugation and edge length, will introduce the first-neighbour stacking constraints depicted in the following subsection.

3.2. Stereochemical constraints and stacking algorithms

We shall not assume any knowledge of the detailed atomic potentials that promote the formation of a given approximant structure. We just observe how it is constructed, its layering system and the constitutive tiling units. Preserving the same units to build up a related structure simply means that most of the set of interatomic forces are the same except for some flexibility that permits the rearrangement. We shall see later in this paper that a rearrangement from an approximant phase to a quasi-crystal involves a small nominal composition change. Conversely, we shall assume that an appropriate composition shift triggers the relevant rearrangement.

The most important characteristic, common to all phases of interest to this work,

is close packing. Therefore, the only requirement that any kind of arrangement of units has to fulfil is to preserve the compactness typical of any metallic alloy. The 3D networks will obviously obey this rule as long as most of the first neighbour distances come close to d_B. Therefore, the following hold:

(i) A structure (approximant or quasi-crystalline) necessarily contains B-type layers (and not only A-type sheets). This obvious rule needs no further comment.

(ii) The succession of A- and B-type layers cannot be random, which imposes constraints on the possible choices of adjacent layers. These first-neighbour constraints are made explicit below.

(iii) The angular shift between successive layers must be specified. Second-neighbour constraints follow, which are given below as well.

The first-neighbour layers that may be associated are listed in table 4. For instance, an A-type layer can only be followed by a B-type layer. Conversely, there is a choice between B* and A sheets for stacking on top of a B layer, etc. When looking at all the possibilities, one may define all the possible starting sequences that contain three layers, the initial one being either of type A or B and the two adjacent ones, i.e. the one below and the one above (third column of table 4).

Second-neighbour constraints arise from (iii) above when a new layer is added to the previous starting sequence. Again, as an example, a layer of type A (or A*)

Table 4. Stacking conditions.

Layer	Possible neighbouring layers	First neighbour sequence	Second neighbour sequence
A	B or B"	BAB B"AB (2) B"AB"	B*|BAB|B* (1) A*|B"AB|B* A*|B"AB"|A*
A*	B* or B"	B*A*B* B*A*B" B"A*B"	B|B*A*B*|B B|B*A*B"|A A|B"A*B"|A
B	B* or A	B*BB* B*BA	B|B*BB*|B A*|B*BB*|B A*|B*BA|B A*|B*BA|B" B|B*BA|B" B|B*BA|B
B*	B or A*	BB*B A*B*B	B*|BB*B|B* B*|BB*B|A B*|A*B*B|B* B*|A*B*B|A B"|A*B*B|B* B"|A*B*B|A
B"	A or A*	A*B"A	B"|A*B"A|B" B"|A*B"A|B B*|A*B"A|B" B*|A*B"A|B

(1) bars like | | limit the sequence formed at the previous step.
(2) BAB" is strictly equivalent to B"AB. For brievity, such sequences are not reported in the table.

cannot join a layer B if a layer A already sits on the opposite side simply because the distance between some A-type layer vertices would be too short. In table 4, we have considered also the B″ layer typical of the λ-$Al_{13}Fe_4$ compound because this specific layer releases this constraint (whereas B′ does not). This layer will play an important role in the following. The 22 possibilities of stacking slabs that take into account the first-neighbour constraints as well as second-neighbour constraints are listed in the fourth column of table 4.

Thus, we have defined a set of rules that govern the stacking of layers to infinity like a cellular automaton. Naturally, diverse structures will build up, depending on whether the 2D sheets are periodic or not on the one hand and the stacking sequence is periodic or not on the other: approximant 3D crystals, 1D aperiodic crystals, 2D aperiodic (decagonal) crystals and 3D aperiodic crystals. In the following, we shall no longer consider the approximant case nor the 1D aperiodic structure produced by stacking 2D periodic networks according to an aperiodic sequence.

Let us thus concentrate first on the decagonal models that may be generated by a periodic stacking of 2D PT. There are basically two ways of doing so, one by stacking A and B planes and the other by introducing as well B″ planes. Considering the first situation, the algorithm may be referred to either an A or a B plane taken as origin. Both cases are considered in table 5(*a*), which presents the various sequences that may be built up to 10 layers with type A and B planes (if Al–Mn alloys are to be accounted for, B′ sheets will substitute for A-type ones; see figure 4). This algorithm satisfies the first- and second-neighbour stacking conditions developed in table 4 and therefore the nature of the layer that may be stacked at a position m above the origin layer is restricted to a limited choice as indicated in table 5(*a*).

We define a coefficient $u_{A,m}$ as the number of distinct possibilities to occupy the layer m when the origin layer is occupied by a sheet of type A. Similarly, the coefficient $u_{B,m}$ will represent the number of possibilities to stack a sheet at position m when the origin layer is a B-type layer. Notice that because an A-type layer is necessarily followed by a B-type layer, the coefficients $u_{A,0}$ and $u_{B,0}$ are shifted by one layer (table 5(*a*)). Now, it is easy to verify that, owing to the constraints given in table 4, these coefficients satisfy the following 'iteration' rules where the iteration runs through successive layers:

$$u_{A,m} = u_{A,m-2} + u_{A,m-3} \tag{3.1}$$

with $u_{A,0} = 1$, $u_{A,1} = 1$, $u_{A,2} = 1$, $u_{A,3} = 2$ the initial coefficients, from which the sequence follows. The sequence also runs such that:

$$u_{A,m} - u_{A,m-1} = u_{A,m-2} - u_{A,m-3}.$$

Also, the 'B' coefficients obey the same rule

$$u_{B,m} = u_{B,m-2} + u_{B,m-3} \tag{3.2}$$

but with initial values $u_{B,0} = 1$, $u_{B,1} = 1$, $u_{B,2} = 2$, $u_{B,3} = 2$. Among all possibilities the number of A or A* layers that may lie on layer m is

$$u_{A,m}^{A/A^*} = u_{A,m-2} + u_{A,m-4} = u_{A,m} - u_{A,m-1} \tag{3.3}$$

while for B and B* layers one has

$$u_{A,m}^{B/B^*} = u_{A,m} - u_{A,m-1}. \tag{3.4}$$

Table 5. (*a*) Stacking algorithms for layers A, A*, B and B*. (*b*) Stacking algorithms for layers A, A*, B, B* and B″.

u_m (referred to A)	u_0	u_1	u_2	u_3	u_4	u_5	u_6	u_7	u_8	u_9	u_{10}
	1	1	1	2	2	3	4	5	7	9	12
(*a*) stacking algorithm	A	- B	- B*	B A*	- B* - B*	B A* - B	- B* - B* A B*	B A* - B - B	- B* - B* A B* - B* - B	B A* - B A B* - B - B	- B* - B* A B* - B* - B* - B* A B*
u_m (referred to B)		u_0	u_1	u_2	u_3	u_4	u_5	u_6	u_7	u_8	u_9
		1	1	2	2	3	4	5	7	9	12

u_m (referred to A)	u_0	u_1	u_2	u_3	u_4	u_5	u_6	u_7	u_8
	1	2	2	4	5	8	12	17	27
(*b*) stacking algorithm	A	B B″	- B* - A*	B A* B″ B″ B* - A - B	B* B* B″ - A - B	B A* B B″ A B* - A - A* B B″ A B*	- B* B* B″ A B* B B″ - A* - B* B″ B - A* - B* A B*	B A* - B - A B B″ - B - A* B″ B* A* B B″ B - A* - B* A B*	- B* B* B″ A B* - B* - A* A B* B″ B - A - B B″ B* - B* A* B B B″ - B

The periodicity of the layering system implies that an A* layer will appear necessarily between two successive A-type layers (B′* between B′ layers in Al–Mn

alloys) in order to cancel the angular shift between layers over the period. An example of such a periodic stacking is ABB*A*B*BA (see table 5(*a*)). Accordingly, the number of layers in a periodic sequence in table 5(*a*) starting on an A layer is necessarily even. Furthermore, the number of independent sequences that may be formed with m layers ($m \leqslant 10$) is readily evaluated from the table 5(*a*).

If one starts from a B-type layer (table 5(*a*)), one has

$$u_{B,m}^{B/B^*} = u_{B,m-2} + u_{B,m-4} = u_{B,m} - u_{B,m-1}. \tag{3.5}$$

For the same reason as above, sequences based on B-type layers will also comprise only an even number of layers. As a matter of fact, there is a single possibility to do so, namely the BB*BB* ... D2 sequence, which contains two layers (table 6). A sequence with two layers such as ABAB is ruled out because of second-neighbour layer exclusion (table 4) as well as a sequence with four layers. Such a sequence will appear, however, after introducing B″ sheets below. Sequences with more layers are possible (table 6), such as the D6 one with six layers and the D8 with eight layers. All D2, D6 and D8 sequences are unique and were already observed experimentally. Conversely, the periodic stacking of 10 layers offers two distinct sequences as table 6 reports but which have not yet been found. Notice that some sequences present mirror planes perpendicular to the stacking direction (space group $P10_5/mmm$) whereas the others do not ($P10_5mc$).

Table 6. Stacking sequences for decagonal phases.

Type of decagonal phase	number of layers	stacking sequence
D 2 (e.g. d-Al-Cu-Co)	2	..BB*.. no mirror
D 4 (e.g. d-Al-Cu-Co)	4	..AB"A*B".. (..*SS*..) ↑ ↑
D 6 (e.g. d-Al-Ni-Mn)	6	..BABB*A*B*.. (..*LL*..) ↑ ↑
D 8 (e.g. d-Al-Fe, d-Al-Cu-Co)	8	..B*BABB*A*B*B.. no mirror
$D10_a$	10	..B*A*B*BB*BB*BAB.. no mirror
$D10_b$	10	..BB*A*B*BB*BABB*.. ↑ ↑

↑ mirror position

Introducing a B″ layer as a possible occupant of layer m changes dramatically the type of structures that may form (table 5(*b*)). The iterative algorithm is now ruled by the relation

$$u_m = 2u_{m-2} + u_{m-3} - u_{m-4} \tag{3.6}$$

with the first three terms being 1, 2 and 2. In this formula, the subscript A was dropped because a type A plane is necessarily included in the sequence if a B″ sheet is also present. Thus, this A plane may always be taken as origin.

Again, periodic sequences will all be composed of an even number of layers. An example of such sequences that was not already pointed out in table 5(*a*) is the D4 sequence with four layers AB″A*B″ (table 6).

Except for the two possible D10a and D10b sequences, which have not yet been observed in real materials, all other stackings fit the experimental data available today.

An important new fact due to the introduction of layer B″ is the existence of long and short segments in the sequences of table 5(*b*), i.e. $\mathcal{L}$ = ABB*A* and $\mathcal{S}$ = AB″A*. Because A-type sheets are actually planar, the length of these segments is well defined. We will demonstrate in the next subsection that these lengths are in the ratio $\mathcal{L}/\mathcal{S} = \tau$ in aperiodic stackings. The point to mention here is that from table 5(*b*) one may have basically three distinct configurations (i) sequences of short slabs, $\mathcal{S}\mathcal{S}\mathcal{S}\mathcal{S}\ldots$, and (ii) sequences of long slabs, $\mathcal{L}\mathcal{L}\mathcal{L}\mathcal{L}\ldots$, both as indicated in table 6, and (iii) interlaced sequences constructed by using both $\mathcal{L}$ and $\mathcal{S}$ slabs.

An example is the D8 sequence presented in table 6. A probably more attractive case is the one that may be built by stacking the two slabs $\mathcal{L}$ and $\mathcal{S}$ according to a Fibonacci scheme. We demonstrate below that this construction is feasible and leads to a calculated composition in agreement with experimental determinations of the composition of the icosahedral phase. We insist again on the point that such a model cannot correspond to an ideal icosahedral phase, which shows the atom number density varying continuously within a certain range when going from one plane to another. Departure from ideal icosahedral point group symmetry is well known, however, in many icosahedral phases, including the thermodynamically stable ones and may therefore be accounted for by our model.

This important specific case is the one that starts with two adjacent slabs $\mathcal{L}$ and $\mathcal{S}$ and therefore is composed of an odd number of five layers. Another sequence $\mathcal{S}\mathcal{L}$, enanthiomorphous to the previous one, may possibly be stacked on top of it, thus leading to a hypothetical D10 decagonal structure, which however has not been observed till now. Looking at table 5(*b*) proves that such a configuration has little probability of occurring as the nominal composition of the structure does not correspond to the appropriate proportion of B″ layers. Indeed, the probability of putting a layer B″ at the sixth position is given by

$$p_6^{B''} = (u_5^{A/A^*}/u_5)(u_7^{A/A^*}/u_7) \tag{3.7}$$

where the coefficients u_m^{A/A^*} have the same meaning as above. From table 5(*b*), one obtains $p_6^{B''} = (3/8) \times (6/17) = 0.132$. Consider now the six equivalent directions of fivefold symmetry along which the stacking must be performed, say on the upper side of an icosahedral cluster. The layers deposited along these directions will interact on edges and vertices of the cluster. This tells us that the probability to lay down B″ layers is vanishingly small ($(p_6^{B''})^6 = 5.4 \times 10^{-6}$).

As a result, the probability to have two successive $\mathcal{S}$ slabs along each of the 12 equivalent fivefold directions of the complete icosahedral cluster is virtually zero and an aperiodic stacking may form with much higher probability than a decagonal phase (with the proviso again that the composition is sharply the right one). There are two interesting conclusions to draw from this point. The first is that the sequence of lengths of the $\mathcal{L}$ and $\mathcal{S}$ slabs naturally follows the Fibonacci series. The length

of the individual segments in icosahedral clusters is examined in figure 6 of the next subsection. But meanwhile the number of individual layers is ruled by the second Lucas series based on $\xi_1^L = 3$ and $\xi_2^L = 4$, which also approximates the golden mean. The second conclusion is that, opposite to the growth of decagonal crystals in the periodic direction, which in the present model entails no difficulty, the growth of an aperiodic stacking necessarily requires removal of many defected layers, which may grow along separate fivefold directions. This may explain why the growth of icosahedral phases is a very slow process [37], for many defects have to be eliminated to achieve icosahedral order.

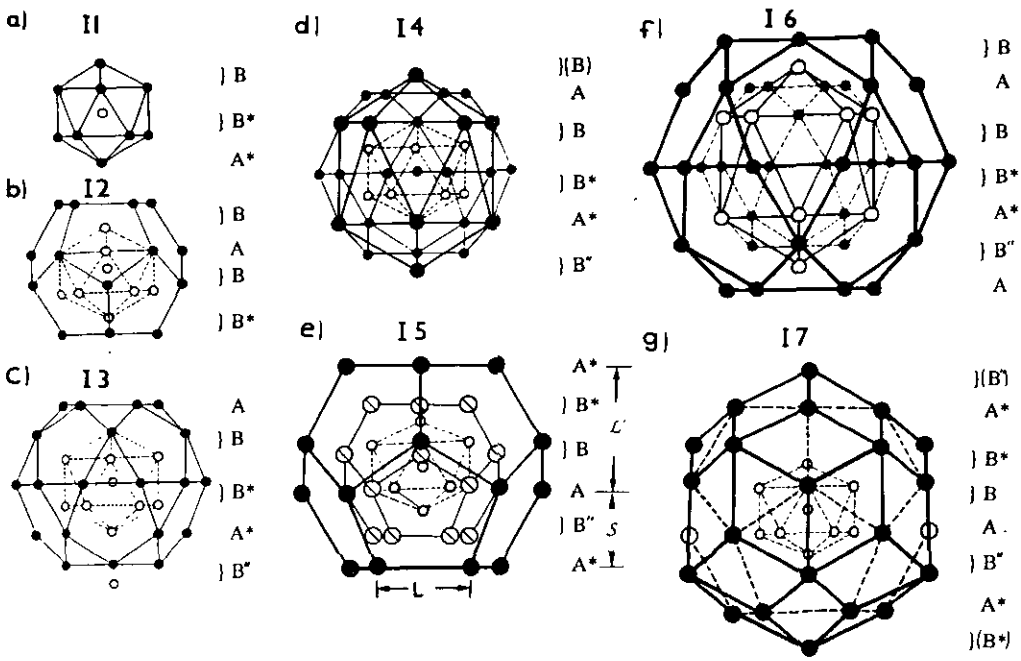

Figure 6. Side views of the 2D cluster models of the icosahedral point group: (*a*) BB*A*-type icosahedral cluster; (*b*) BABB*-type dodecahedral cluster; (*c*) ABB*A*(B″)-type icosadodecahedral cluster (with broken lines: icosahedral kernel); (*d*) (B)ABB*A*B″-type icosahedral cluster (thick lines) including an ABB*A*(B″) icosadodecahedral cluster (thin lines) and a BB*A* icosahedral kernel; (*e*) the A*B*BAB″A*-type dodecahedral cluster (thick lines) including a B*BAB″ dodecahedral cluster (thin lines) and a (B*)BA(B″) icosahedral cluster kernel (broken lines); (*f*) BABB*A*B″A-type icosadodecahedral cluster (thick lines) including a (B)ABB*A*B″ icosahedral cluster (thin lines) and an ABB*A*(B″) icosadodecahedral cluster (broken lines); and (*g*) (B″)A*B*BAB″A*(B*)-type rhombic triacontahedral cluster (thick lines) including an A*B*BAB″A* dodecahedral cluster (broken lines) and a (B*)BA(B″) icosahedral cluster (thin lines).

The change from a periodic to a quasi-periodic stacking of atomic slabs is basically related to a composition change. Indeed, an odd number of layers requires a change in the number of A-type layers (B′ in Al–Mn alloys) relative to that of B and B* ones. The introduction of a B″-type layer is specifically able to achieve such a variation. More precisely, a Fibonacci stacking will be characterized by a relative abundance

$(\tau/3 + 1/2)/\tau^2 \simeq 0.39$ of A layers (or B'), which falls between the values of 1/2 appropriate to the D4 stacking and 1/3 for the D6 sequence. If the model is designed for Al–Mn alloys by comparing to the β-Al_6Mn compound, the aperiodic stacking will contain fewer Mn atoms than the decagonal one because the number of B' layers, which carries only Al atoms, will increase. Opposite to this, for the Al–Mn–Ni alloys, the aperiodic model will require a higher proportion of A-type layers than the decagonal case and therefore will contain more Ni atoms. Section 5 will argue in more detail on this point.

3.3. Construction of clusters with the icosahedral point group symmetry

According to the previous section, models constructed by stacking atomic sheets of A, B and B'' type may be able to account for either decagonal ordering or for defected icosahedral order. In the present section, we construct the first four clusters of the icosahedral point group and show that they correspond indeed to the icosahedral monograins known so far. We focus on fragments of layers of the types already introduced and restrict ourselves to those atoms which occupy the vertices of the relevant cluster centred at the origin of the lattice. The very same clusters form around all fivefold coordinated nodes of the initial A-type layer of the sequence. Layers of infinite extension will propagate the same order along all 12 equivalent directions of fivefold symmetry. We shall not, however, assume that this model is directly related to the actual growth mechanism of quasi-crystals despite the fact that the outermost shells actually fit the real crystal growth morphologies of stable icosahedral phases.

Figure 6 presents the series of clusters with the constitutive layers shown. The stacking direction is vertical in this figure. Refer to table 7 for the labelling of stacking sequences. The smallest cluster that can be obtained (figure 6(*a*)) is the icosahedron I1 (I because the central polyhedron belongs to the icosahedral cluster group, 1 because it is the first one in the hierarchy of figure 6). It is formed by an atom at the centre surrounded by 12 other atoms. This kind of icosahedral cluster has been observed in many crystalline compounds, for instance, in Al–Mn [31] and in Al–Mo [38] alloy systems. The I1 cluster has eight variants (namely, $i_1 \ldots i_8$) with different generating sequences as given in table 7.

Next in the series comes the dodecahedral I2 cluster (figure 6(*b*)). This cluster can be constructed in two ways, by using either a B*BAB stacking or a B*BAB'' stacking (table 7). Then the smallest icosadodecahedral cluster (figure 6(*c*)) can only be constructed in one way, with stacking sequence ABB*A*B'' (table 7). Up to this stage, these clusters are not specific and may be found in both icosahedral and decagonal phases since they all contain a fragment of the $\mathcal{L}$ segment, i.e. the slab BB*.

Clusters with edge length $d_A = 4.55$ Å $= \tau d_B$ will form at the next step of the construction, although it is important to insist again that this view is artificial and is elaborated only to simplify the presentation: A-type layers already constituting the previous clusters have the same edge length as the new ones and the vertices of the layers shared by successive shells already exist. For clarity, they are just not drawn. The icosahedral I4 cluster has six variants (table 7). These variants can be distinguished into two groups, one originating from the i_1 cluster (the 'kernel') and the other from the i_5 cluster (table 7). One of its models with stacking sequence (B)ABB*A*B* is given in figure 6(*d*) (hereafter, the notation (□) indicates that only a part of the corrugated layer in terms of thickness t (see figure 5) belongs

Table 7. (*a*) Stacking sequences for four types of cluster models. -->, sequences which will lead to a perfect stacking (Fibonacci stacking sequence). B, B* and B'' are corrugated layers and therefore some of the atoms that are in the upper and lower layers do not belong to the cluster under consideration. When such a layer is introduced, it is referred to by brackets ().

cluster model	stacking sequence
I 1 (τ^{-1}I4II-icosahedron)	i_1 - BB*A* i_2 - (B*)BA(B") i_3 - (B*)BA(B) i_4 - A*B"A(B") i_5 - A*B"A(B) i_6 - B"A*B* i_7 - B*B(B*) i_8 - BB*(B)
I 2 (τ^{-1}I5II-dodecahedron)	1) I 2_1-type -B*BAB 2) I 2_2-type - B*BAB"
I 3 (τ^{-1}I6II-icosadodecahedron)	ABB*A*(B")
τ^{-1}I7II-rhombic triacontahedron	no sequence can be generated in such conditions
I 4 (I4II-icosahedron)	1) I 4_1-type - (B)ABB*A*B* --> (B)ABB*A*B" --> (B")ABB*A*B* --> (B")ABB*A*B" 2) I 4_2-type --> (B*)BAB"A*B* - (B*)BAB"A*B"
I 5 (I5II-dodecahedron)	--> A*B*BAB"A*
I 6 (I6II-icosadodecahedron)	1) I 6_1-type --> BABB*A*B"A 2) I 6_2-type - BB*A*B"AB"A* - AB"A*B"AB"A*
I 7 (I7II-rhombic triacontahedron)	--> B*A*B*BAB"A*B* - B*A*B*BAB"A*B" --> B"A*B*BAB"A*B* - B"A*B*BAB"A*B"

to the polyhedron). The vertex atoms of this icosahedral shell are located on top of the icosadodecahedral I3 pentagon faces and constitute the well known Mackay icosahedron [39]. The dodecahedral I5 cluster (figure 6(*e*)) can only be constructed by one sequence A*B*BAB''A*, which originates from the same i_2 variant of the I2 cluster. In the icosadodecahedral I6 case, the cluster has three variants (table 7). They are built on two distinct clusters, i_1 and i_4. These clusters are different from the ones in the smallest I3 model (i.e. i_2 and i_3). One I6 cluster with sequence BABB*A*B''A is schematized in figure 6(*f*) (the central kernel i_1 is missing and only vertex atoms are drawn). This cluster forms around the I4 cluster of figure 6(*d*) and represents the main cluster pointed out by high-dimensional crystallographic analysis of the Al–Mn icosahedral phase [40]. The rhombic triacontahedron, cluster I7, has four variants. We show in figure 6(*g*) one of the four variants, namely (B'')A*B*BAB''A*(B*). This variant surrounds the dodecahedral I5 cluster schematized in figure 6(*e*) but not drawn in figure 6(*g*). This I7 cluster is the triacontahedral cluster of atoms characteristic of Al–Cu–Li alloys [41] and resembles the cluster used in the model proposed by Duneau and Oguey [21]. It was recognized in the structure of the Al–Cu–Li icosahedral phase obtained by a high-dimensional crystallographic approach [42].

To conclude this subsection, it is clear that perfect icosahedral ordering cannot

be produced by any sequence containing only the $\mathcal{L}$ and $\mathcal{S}$ segments. Nevertheless, a stacking of both slabs that is arranged according to the Fibonacci algorithm closely approaches the atomic arrangement observed in icosahedral phases. In the next section, we shall refer to this type of network as the pseudo-icosahedral phase. The lengths are then naturally in the ratio $\mathcal{L}/\mathcal{S} = \tau$. The Mackay icosahedron, which was often recognized as a basic constitutive block of Al–transition metal (e.g. Al–Mn, Al–Cu–Fe) icosahedral phases, is clearly present in the stackings studied here. In the Al–Li–Cu icosahedral phase, the equivalent building block is the so-called 'soccer ball' constructed by an I7 cluster surrounding an I5 dodecahedron, which also arises in the appropriate stacking. On the contrary, in the decagonal phase complete clusters at the highest hierarchy level, i.e. I4 to I7, cannot form because $\mathcal{L}$ and $\mathcal{S}$ segments cannot become adjacent to each other. This argument points out the most significant difference between the two types of quasi-crystals.

4. Relative number of tiling units

There are two isostructural decorations of the Penrose tiling (PT) that are used to describe the quasi-periodic structure of the decagonal and pseudo-icosahedral quasi-crystals. One pattern is constructed by f and t tiling units [43] (hereafter, called the PT1 pattern) and the other is constructed by v, t and c units [7] (hereafter, the PT2 pattern). We reproduce these patterns with a fivefold symmetry centre in figures 7(*a*) and 8(*a*). The atomic decorations of the PT1 and PT2 patterns are deduced from the β-Al_6Mn and $\phi 1$ structures, respectively (see section 5 for details). The PT1 pattern is generated by tiling the plane with f and t units and applying the matching rules introduced by de Bruijn [43]. It can be transformed to the PT2 pattern by replacing the f and t units (with no atomic decoration) by the v, t and c units according to the line decoration schematized in the left side of figure 8(*a*) (the dots indicate the 'pole' vertices) [44].

We use the inflation rules [45] to calculate the relative abundance number F_i of a tiling unit (i = f, t, v and c) in both PT patterns. Consider first a single tiling unit, either the fat rhombus (f) of the PT1 pattern (unit of order $n = 0$ in figure 7(*b*)) or the convex pentagon (v) of the PT2 pattern (unit of order $n = 0$ in figure 8(*b*)). The edge length $\tau^n d_0$ of the tiling unit increases (d_0 is kept constant) with inflation according to the inflation order number $n = 0, 1, 2, 3, \ldots$ or $n = 0, 2, 4, 6, \ldots$ for the PT1 or PT2 patterns, respectively. In the PT1 pattern, the total number ξ_n^f of f units increases with the inflation order number n like the odd-order coefficients of the Fibonacci series, i.e. $\xi_n^f = \xi_{2n-1}^F$. For instance, at step number 2 of the inflation, there are five f units while there are 13 at the next step (figure 7(*b*)). The number of t units increases like the even-order terms of the Fibonacci series, i.e. $\xi_n^t = \xi_{2n-2}^F$. Therefore, the relative number of f units $F_f = \xi_n^f/(\xi_n^t + \xi_n^f)$ approximates the inverse golden mean τ^{-1} like the Fibonacci ratio $\xi_{2n-1}^F/(\xi_{2n-2}^F + \xi_{2n-1}^F)$. Accordingly, the relative abundance of the thin rhombus (t) is $F_t = 1 - F_f = \tau^{-2}$. Meanwhile, in the PT2 pattern, the relative numbers of convex pentagons (v), thin rhombuses (t) and concave pentagons (c) are respectively given by $F_v : F_t : F_c = \tau^{-1} : \tau^{-3} : \tau^{-4}$.

5. Model quasi-crystal for Al–Mn–(Ni) alloys and experimental tests

Atomic decoration models were sometimes proposed as an interpretation of

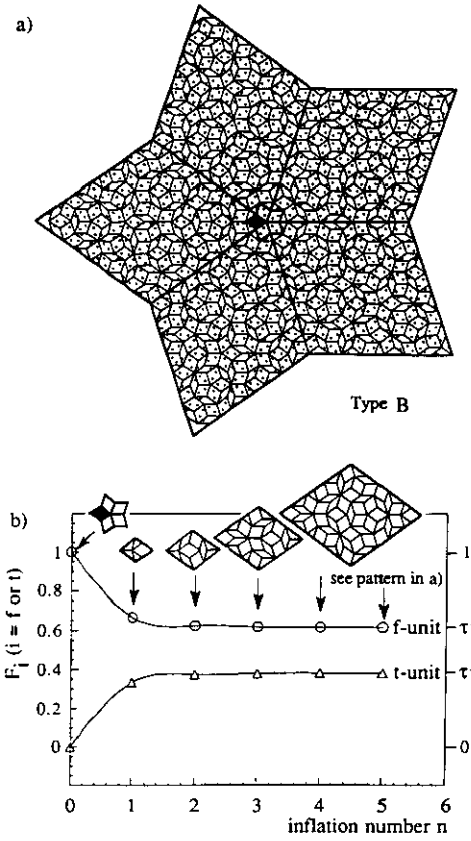

Figure 7. (*a*) Penrose tiling PT1 constructed by f- and t-rhombuses. The atomic configuration is laid out according to the B layer in β-Al_6Mn. (*b*) Relative number F_i of fat f- and thin t-rhombuses versus inflation order number n of the unit edge length $\tau^n d_0$, with d_0 the initial edge length of the sublattice.

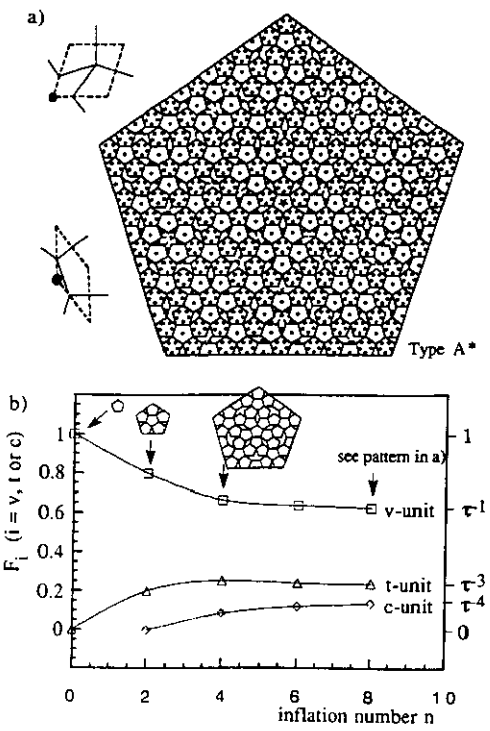

Figure 8. Penrose tiling PT2 constructed by v-pentagons, t-rhombuses and c-pentagons. The atomic configuration is taken from the A layer in ϕ_1-$Al_{60}Mn_{11}Ni_4$. (*b*) Relative number F_i of convex v-pentagons, thin t-rhombuses and concave c-pentagons versus inflation order number n of the unit edge length $\tau^n d_0$, with d_0 the initial edge length of the sublattice.

experimental results [46,47], but the most advanced designs were built on a comparison with crystal references. In order to substantiate the general model proposed in the first part of this paper, we shall also build a specific model for a quasi-crystalline phase of given composition, starting from atomic position data on a related crystal. For illustration, let us first select two parent structures: ϕ1-$Al_{60}Mn_{11}Ni_4$ and β-Al_6Mn. This choice is made for two reasons. First, the Al_6Mn crystal may be formed by crystallization of its related quasi-crystal [48]; and secondly, their lattices (perpendicular to a pseudo-fivefold axis) can be constructed with the help of f, t, v and c units (figure 4). In fact, their structure units can be used to generate a quasi-periodic PT1 pattern or alternatively a PT2 pattern owing to the lattice transformation rules introduced by Henley [44] (see units schematized in left side of figure 8(*a*)). We will explain this point of view for the Al–Mn alloy with the PT1 pattern (section 5.1.1) and for an Al–Mn–Ni alloy with the PT2 pattern (section 5.1.2).

5.1. Composition of the decagonal phase

5.1.1. Al–Mn–Ni decagonal phase. Using the atomic decoration of the subtiling elements in the $\phi 1$ phase, an atomic decoration of the PT2 pattern is generated (figure 8(*a*)). This 2D PT pattern can be further lifted to a 3D model by assuming that the sequence in the third dimension follows the sequence of the $\phi 1$ phase, i.e. $d_3 = 12.5$ Å (periodic distance in the decagonal d-Al–Ni–Mn phase [49]) and sequence ABB*A*B*B (table 3). This 3D model is in fact packed by five subunit polyhedra such as the ones shown in figure 9. The first three units V, V* and P are exactly the same as the units constructing the $\phi 1$ phase. Note that the capital letters V, V* etc., label the 3D tiling units with 2D basis tiles denoted v, v*, etc., respectively. The other two units C and C* come from the space left open between the previous ones when constructing the PT. The relevant atomic decoration is obtained on the one hand by preserving the fivefold symmetry around the centre marked by a star in figure 8(*a*), i.e. applying the 10-fold symmetry operation. On the other hand, the $\phi 1$ phase exhibits a mirror perpendicular to the b axis, which we shall preserve in the decagonal structure model, thus going to the $P10_5/mmm$ space group symmetry. Since this 3D model is based on the low-energy atomic configuration of the stable $\phi 1$ phase, the occupancy factors ψ for each site are supposed to be identical to the ones in the initial structure of the $\phi 1$ phase. Here $\psi_{Xj} = 1$ for the occupancy factor of element X (X = Al, Mn or Ni) and atomic site number j (j = 1, 2, 3, ...). To calculate the composition of the decagonal phase in the Al–Mn–Ni system, we count the number of atoms of each species present in each polyhedral unit V, T or C. From section 4, the relative abundance of units v, t and c in the PT pattern is $F_v : F_t : F_c = \tau^{-1} : \tau^{-3} : \tau^{-4}$, which is also the one for the units in 3D. The general formula that gives this composition can be written as:

$$F_X^d = \psi_{Xj} \sum_{i=V,V^*,\ldots} F_i X_i$$
$$= \psi_{Xj}[F_v/2(X_V + X_{V^*}) + F_t X_T + F_c/2(X_C + X_{C^*})] \qquad (5.1)$$

where F_X^d is the number of atoms X present in the model decagonal structure and X_i is the number of atoms X counted in each polyhedral unit of type i (i = V, V*, T, C and C*). In this case, the calculated composition for a perfectly ordered decagonal phase is $Al_{78.58}Mn_{16.50}Ni_{4.92}$ (at.%). This composition is close to the composition of the $\phi 1$ phase ($Al_{79.49}Mn_{15.38}Ni_{5.13}$), which is characterized by $F_v : F_t = 4:2$. Assuming that the pattern presented in figure 1(*a*) is suitable for the isostructural O_1 phase with $F_v : F_t : F_c = 16:6:4$, the composition would be $Al_{78.52}Mn_{16.56}Ni_{4.91}$. In comparison, the experimental composition of the O_1 phase determined by optimizing alloy compositions (see next subsection) is around $Al_{79.8}Mn_{14.8}Ni_{5.4}$. It is remarkable that a change in the relative number of tiling units, which entails a minute change of composition (table 8), triggers the structure construction into the true decagonal phase instead of the approximant structure, $\phi 1$ phase. The calculated compositions of the decagonal and O_1 phase are almost the same within 0.1%. The reversible phase transitions that are often observed between quasi-crystals and their approximants [1,3,50] may accordingly be related to the temperature dependence of the solubility of chemical species in the high-temperature quasi-crystal.

5.1.2. Al–Mn decagonal phase. The structure of β-Al_6Mn consists of four layers, namely B′BB′B* as already mentioned. This scheme cannot be directly applied to

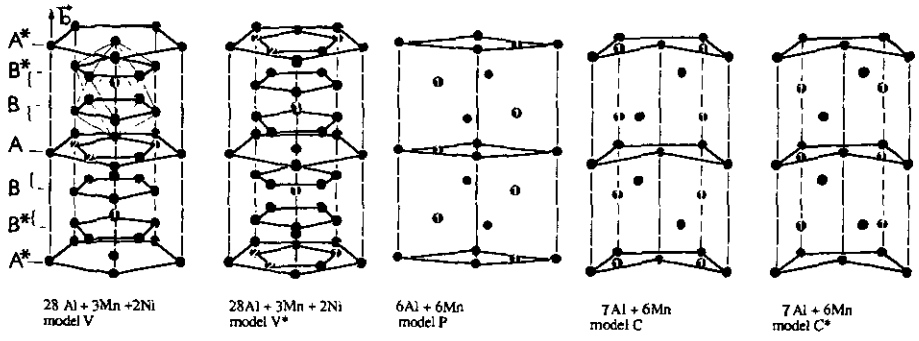

Figure 9. Set of 3D tiling units suitable for the decagonal phase of the Al–Mn–Ni system with $d_3 = 12.5$ Å. The atoms marked 1 and 2 are Mn and Ni respectively, and full circles are Al atoms. The V* and C* units have the same atomic content as the V and C units, respectively.

Table 8. *Experimental and calculated* compositions for quasi-crystalline and crystalline phases in Al–Mn–Ni and Al–Mn alloy systems.

Phases	Experimental composition		Calculated composition	
	Al-Mn-Ni alloys	Al-Mn alloys	Al-Mn-Ni alloys	Al-Mn alloys
Decagonal phase	$Al_{79.82}Mn_{14.83}Ni_{5.35}$ (1) (this work)	$Al_{77}Mn_{23}$ (ref. 38)	$Al_{78.58}Mn_{16.50}Ni_{4.92}$	$Al_{77.4}Mn_{22.6}$
Icosahedral phase	$Al_{80.75}Mn_{13.75}Ni_{5.5}$ (2) (this work)	$Al_{79.6}Mn_{20.4}$ (ref. 42)	$Al_{77.34}Mn_{16.72}Ni_{5.94}$	$Al_{79.4}Mn_{20.6}$
	$Al_{80}Mn_{13}Ni_7$ (2) (ref. 53)	$Al_{79.5}Mn_{20.5}$ (ref. 43)		
ϕ1 phase	$Al_{79.49}Mn_{15.38}Ni_{5.13}$ (ref. 33)		$Al_{79.49}Mn_{15.38}Ni_{5.13}$	
isostructural O1-phase	$Al_{79.82}Mn_{14.83}Ni_{5.35}$ (3) (this work)		$Al_{78.52}Mn_{16.56}Ni_{4.91}$	

1- As quenched state containing an almost decagonal phase.
2- As quenched state containing a mixture of decagonal, crystalline and icosahedral phases
3- As annealed state (3 hours at 825°C) containing several other minority crystalline phases.

the Al–Mn decagonal phase because the repetition distance along the 10-fold axis is too long, i.e. 12.4 Å, suggesting that six layers are needed. We thus select a sequence B'BB*B'B*B, which shows mirror planes on B' sheets in accordance with some electron diffraction results [5]. Applying the atomic decoration of each tiling element in the β-Al_6Mn (figure 10) structure to a PT1 pattern will give for example the configuration given in figure 7(*a*). To estimate the composition of this decagonal phase, we calculate the proportion of each layer (B' or B and B*) present in the sequence B'BB*B'B*B and we count the number of atoms X occupying each layer. With $F_l: F_t = \tau^{-1}: \tau^{-2}$ (from section 3), the proportion of layer l (l = B or B') in the sequence BB*B'B*BB', $F_B: F'_B = 2/3: 1/3$ and the number of atoms X in layer l, $N^B_{Al}: N^B_{Mn} = \tau: 1$ and $N^{B'}_{Al}: N^{B'}_{Mn} = 3.618: 0$, the general formula becomes

$$F^d_X = \sum F_l N_X = (N^B_X F_B + N^{B'}_X F_{B'}) \tag{5.2}$$

where F^d_X is the relative abundance of atomic species X in the Al–Mn decagonal phase.

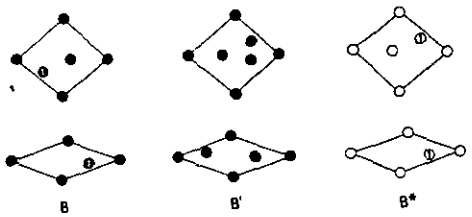

Figure 10. (*a*) Two-dimensional subtiling elements corresponding to the layers B, B' and B* of β-Al_6Mn with 1 indicating Mn atoms (see also figure 4).

The composition that can be deduced from this formula is $Al_{77.4}Mn_{22.6}$. This composition is very close to the experimental one $Al_{77}Mn_{23}$ as reported by Daulton *et al* [51].

5.2. Composition of the pseudo-icosahedral phase

In this section, we use the 2D Penrose tilings PT1, $F_f: F_t = \tau^{-1}: \tau^{-2}$ (figure 9), and PT2, $F_v: F_t: F_c = \tau^{-1}: \tau^{-3}: \tau^{-4}$ (figure 8), and the perfect Fibonacci stacking sequence ($N_{\mathcal{L}}/N_{\mathcal{S}} = \tau$) to calculate the composition of the pseudo-icosahedral model in order to make comparisons with data available on the icosahedral phases existing in the Al–Mn and Al–Mn–Ni alloy systems. The example below is given for the case of Al–Mn–Ni alloys.

First, we calculate the number of atoms in each layer l (l = A or B), (N_X^l). The number of atoms X = Al, Mn or Ni in layer A are:

$$N_{Al}^{A} = \tfrac{1}{2}(2.5 + 3.5)F_v + 1F_t + \tfrac{1}{2}(1.5 + 1.5)F_c = 2.309$$
$$N_{Mn}^{A} = \tfrac{1}{2}(1)F_v + 1F_t + \tfrac{1}{2}(2)F_c = 0.691$$
$$N_{Ni}^{A} = \tfrac{1}{2}(2)F_v = 0.618$$

whereas in layer B:

$$N_{Al}^{B} = \tfrac{1}{2}(5.5 + 5.5)F_v + 1F_t + 1F_c = 3.781$$
$$N_{Mn}^{B} = \tfrac{1}{2}(0.5 + 0.5)F_v + 1F_t + 1F_c = 0.691$$
$$N_{Ni}^{B} = 0F_v = 0.$$

Secondly, we calculate the relative number F_l^w of layers l stacked in a segment w of the sequence of tiles $w = \mathcal{L}$ or $\mathcal{S}$ ($\mathcal{L}$ = ABB*A* and $\mathcal{S}$ = AB*A*). We obtain the ratio $F_A^{\mathcal{L}}: F_B^{\mathcal{L}} = 1/3{:}2/3$ and $F_A^{\mathcal{S}}: F_B^{\mathcal{S}} = \tfrac{1}{2}{:}\tfrac{1}{2}$. Thirdly, we calculate the relative abundance $F_w^{\mathcal{F}}$ of segments w in the perfect Fibonacci ($\mathcal{F}$) stacking, yielding the ratio $F_{\mathcal{L}}^{\mathcal{F}}: F_{\mathcal{S}}^{\mathcal{F}} = \tau^{-1}: \tau^{-2}$. Then, the general formula can be rewritten as

$$F_X^i = \sum F_w^{\mathcal{F}} \sum F_l^w N_X^l = F_{\mathcal{L}}^{\mathcal{F}}(N_X^A F^{\mathcal{L}} + N_X^B F_B^{\mathcal{L}}) + F_{\mathcal{S}}^{\mathcal{F}}(N_X^A F_A^{\mathcal{S}} + N_X^B F_B^{\mathcal{S}}) \qquad (5.3)$$

where F_X^i is the relative abundance of element X in the pseudo-icosahedral phase. The calculated compositions are i-$Al_{77.34}Mn_{16.72}Ni_{5.94}$ (at.%) and i-$Al_{79.4}Mn_{20.6}$ (at.%) (table 8). The composition calculated for the Al–Mn–Ni icosahedral phase is slightly

different from the composition $Al_{80.75}Mn_{13.75}Ni_{5.5}$ measured in this work (see next subsection) and $Al_{80}Mn_{13}Ni_7$ as reported in [52]. Note that these experimental determination were performed on specimens consisting of a mixture of crystalline, decagonal and icosahedral phases. Although close to it, they do not represent the true composition of the icosahedral phase.

In contrast with the decagonal phase, which grows in the same alloy system Al–Mn–Ni, the icosahedral phase needs more Ni atoms than the decagonal phase. The Fibonacci sequence increases the number of layers A by a factor $\tau^4/3$ with respect to the periodic sequence ABB*A*B*B. Since Ni atoms are found only in layer A, their presence thus favours the formation of the icosahedral phase. For the Al–Mn case, the calculated composition $Al_{79.4}Mn_{20.6}$ is almost exactly the same as the composition $(Al/Si)_{79.1}Mn_{20.9}$ calculated by Duneau and Oguey [21] or the experimental composition $Al_{79.5}Mn_{20.5}$ as reported for Al–Mn icosahedral phases that contain no silicon [22, 53].

5.3. Experimental data on the Al–Mn–Ni decagonal phase

The validity of our approach may be tested experimentally by scanning the structures that form in these alloy systems, for instance in the Al–Mn–Ni alloy, as functions of composition. Note that the real compositions of the decagonal phase [49] as well as of the icosahedral phase [52] have not yet been determined. To this end, let us first consider three ratios of polyhedral tiling units $F_V : F_T : F_C$ as follows:

(A) 0.5:0.3:0.2 corresponding to a composition $Al_{75.0}Mn_{20.1}Ni_{4.9}$

(B) 0.651:0.218:0.131 corresponding to a composition $Al_{79.82}Mn_{14.83}Ni_{5.35}$

(C) 0.81:0.11:0.08 corresponding to a composition $Al_{80.75}Mn_{13.75}Ni_{5.5}$

These ratios span an overestimated range with respect to the relative number of units in the PT2 pattern, so that the results will be more noteworthy for structure analysis.

Alloys of nominal composition as indicated above were prepared in an induction melting furnace under inert helium atmosphere. In order to study the phase stability versus the cooling rate, ribbon samples were prepared by the melt spinning technique on a rotating copper wheel at two quenching rates produced either by a low quenching wheel speed of 12 m s^{-1} for the samples denoted M_1 or by a high quenching wheel speed of 40 m s^{-1} for the samples denoted M_2 (M = A, B or C as defined above). Their stabilities have also been studied by differential scanning calorimetry (DSC) with controlled heating and cooling rates (5 °C min^{-1}). Figures 11 and 12 present the x-ray diffraction patterns of all quenched samples. Only the alloy B, which corresponds to the exact calculated nominal composition of the d phase, shows a pure decagonal-like diffraction pattern (figure 11). The formation of this d phase is almost independent of the quenching rate. As indexed in the diffractogram (figure 12), only a small amount of primitive hexagonal ϵ phase (a = 17.8 Å and c = 12.5 Å) is observed in the sample prepared at the highest quenching rate. In fact, the d phase is not stable. A transformation peak begins to appear at about 650 °C on the DSC curve (figure 13). After annealing for 3 h at 825 °C and slow cooling to room temperature, the sample gives a diffraction pattern characteristic of a few crystalline phases (not shown here). From [49] the transmission electron microscopy results obtained on an alloy of composition identical to that of the $\phi 1$ phase show that a decagonal phase

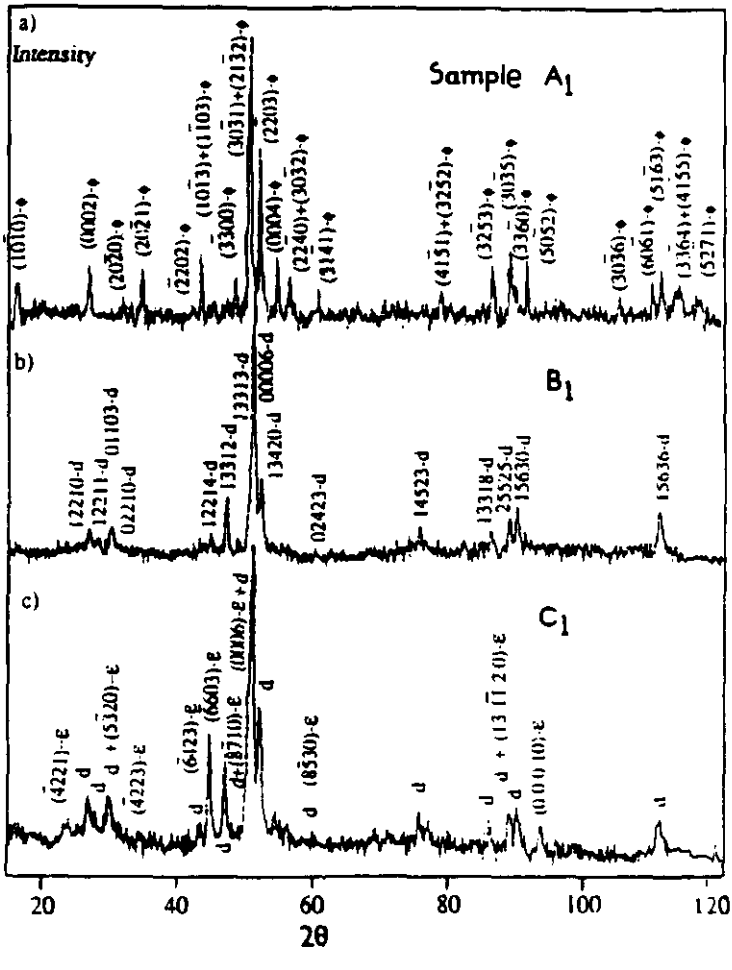

Figure 11. X-ray diffraction patterns of melt-spun samples quenched at 12 m s^{-1}: (*a*) $Al_{75.5}Mn_{20.1}Ni_{4.9}$ (at.%), alloy A—sample A_1; (*b*) $Al_{79.02}Mn_{14.93}Ni_{6.35}$ (at.%), alloy B—sample B_1; and (*c*) $Al_{80.75}Mn_{13.75}Ni_{5.5}$ (at.%), alloy C—sample C_1. See [56] for decagonal indexing.

is produced in the quenched samples but, after the authors, this phase transforms to a mixture of several approximant phases when a long-term annealing is performed. In our annealed sample, more than one crystalline phase is contained, but with the $\phi 1$ phase as the major constituent. One of the other crystalline phases is an orthorhombic phase isotypic to the O_1 phase [54] (see figure 11(*a*)), space group $Bbm2_1$, cell parameters $a = 22.5$ Å, $b = 12.5$ Å and $c = 30.44$ Å.

When reducing the f_V ratio (alloy A), the d phase can be formed only at a high quenching rate (figure 12(*a*)). It is transformed to a crystalline phase ϕ with cell parameters $a = 7.59$ Å and $c = 7.83$ Å, space group $P6_3/mmc$ isotypic with the ϕ-$Al_{10}Mn_3$ hexagonal phase [55] upon heating up to 590 °C (figure 13(*a*)). At low quenching rate, the amount of the d phase is negligible (figure 1(*a*)). When increasing the f_V ratio (alloy C), the d phase seems to be more stable at room temperature.

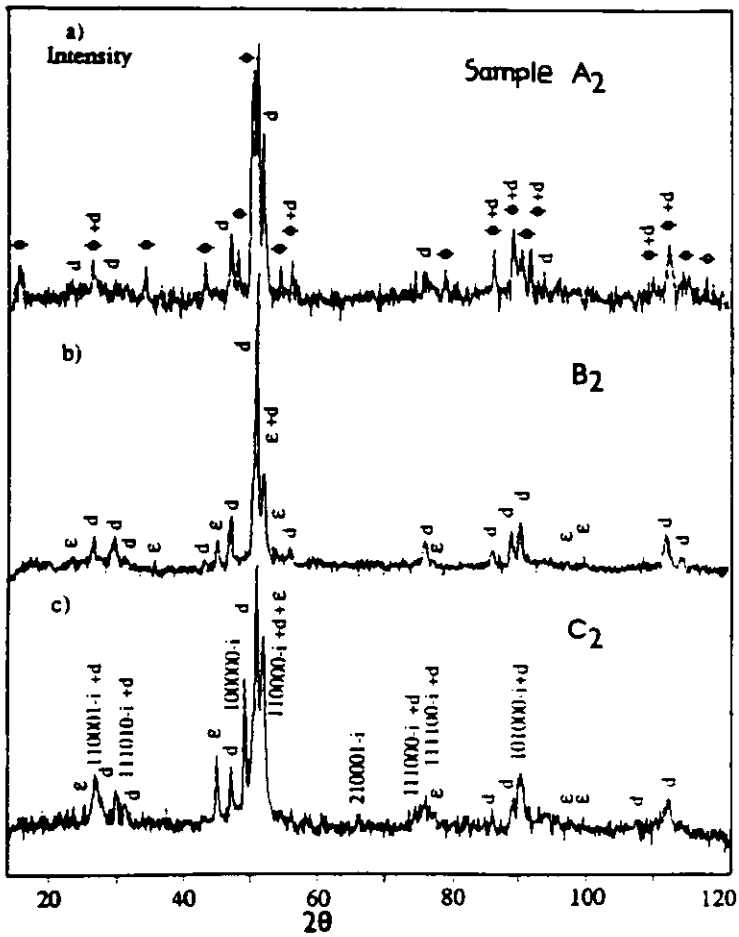

Figure 12. Same as figure 11 but for melt-spun samples quenched at 40 m s^{-1}. See [57] for icosahedral indexing.

Although it coexists with the ϵ phase (figures 11(*c*) and 12(*c*)), no transformation peak can be observed in the DSC curve (figure 13(*c*)). The diffractogram of this d phase can be relevant either to a microcrystalline state or to a stable decagonal phase, but referring to its irregularly shaped and quite broadened peaks, it most probably refers to a microcrystalline rather than quasi-crystalline state. If the transformation exists, it may be very sluggish so that the variation of enthalpy ΔH becomes too small to be detected. This explains why the endothermic signal of the alloy B (figure 13(*b*)) is in fact detected at crystal–crystal phase transitions. The decagonal → approximant transition may take place before this endothermic peak. In addition, a metastable icosahedral phase [52] has been found in the higher quenching rate sample of the same alloy (figure 12(*c*)).

6. Conclusions

A detailed classification scheme in 1D, 2D and 3D real space is proposed for the

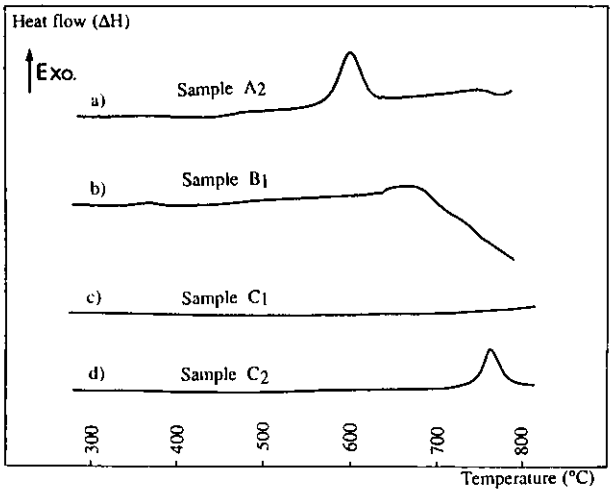

Figure 13. Differential scanning calorimetry (DSC) curves (heating rate 5 °C min^{-1}) for melt-spun samples: (*a*) alloy A—sample A2, 40 m s^{-1}; (*b*) alloy B—sample B_1, 12 m s^{-1}; (*c*) alloy C—sample C_1, 12 m s^{-1}; and (*d*) alloy C—sample C2, 40 m s^{-1}.

approximant phases, fivefold symmetry and 10-fold symmetry quasi-crystals. This scheme is based on the close relationship between the structure of the approximant and the quasi-crystalline phases. It may also be applicable to other crystalline phases and quasi-crystalline phases by packing other subtiling units.

Referring to the construction of 3D cluster models of the icosahedral group in simulated layering systems, we conclude that pseudo-icosahedral quasi-crystals may be built with two layers (or more) stacked along a fivefold axis as the decagonal quasi-crystals do. However, this time the stacking sequence is generated with the atomic layers grouped in short and long segments reproduced aperiodically. This relates the pseudo-icosahedral phase and the decagonal phase to a unique stacking scheme of atomic layers: variants depend on the details incorporated in the layering system and basically on the nominal composition. We suggest that the decagonal or approximant structures will form when a centrosymmetric position is present in the stacking whereas the icosahedral structure will form if the stacking sequence contains a non-centrosymmetric origin.

This way of describing the structure allows us to infer the structure of any phase (approximant as well as decagonal or icosahedral) by construction of 3D model structures based on a known crystalline phase (if it exists) whose composition is nearby. This approach is applied to the Al–Mn–Ni and Al–Mn alloy systems. We have shown that the formation of specific quasi-crystalline phases depends mainly on the relative proportion of convex pentagons with respect to concave pentagons and rhombic tiling elements. The suitable ratio for the quasi-crystalline phase corresponds to that obtained for a perfect Penrose tiling, namely $F_f: F_t = \tau^{-1}: \tau^{-2}$ and $F_v: F_t: F_c = \tau^{-1}: \tau^{-3}: \tau^{-4}$. The calculated compositions are in agreement with the experimental results.

Acknowledgments

We are grateful to Dr Chuang Dong for fruitful discussions and to Dr Michel Duneau for his most helpful criticism of the manuscript.

References

[1] Audier M and Guyot P 1990 *Proc. 3rd Int. Meeting on Quasicrystals (Mexico)* ed J Yacaman *et al* (Singapore: World Scientific) p 288
[2] Audier M, PLaunois P, Denoyer F, Dong C and Dubois J M 1990 *Microsc. Microanal. Microstruct.* **1** 417
[3] Launois P, Audier M, Denoyer F, Dong C, Dubois J M and Lambert M 1990 *Europhys. Lett.* **13** 629
[4] Dong C, Dubois J M, Kang S S and Audier M 1991 *Phil. Mag.* **65** 107
[5] Bendersky L 1985 *Phys. Rev. Lett.* **55** 1461
[6] Shechtman D, Blech I, Gratias D and Cahn J W 1984 *Phys. Rev. Lett.* **53** 1951
[7] Penrose R 1974 *Bull. Inst. Math. Appl.* **10** 266
[8] Steurer W and Kuo K H 1990 *Phil. Mag. Lett.* **62** 175
[9] He L X, Wu Y K, Meng X M and Kuo K H 1990 *Phil. Mag. Lett.* **61** 15
[10] Kumar V, Sahoo D and Athithan G 1986 *Phys. Rev.* B **34** 6924
[11] Nicol A D L 1953 *Acta Crystallogr.* **6** 285
[12] Black P J 1955 *Acta Crystallogr.* **8** 43
[13] Chattopadhyay K, Lele S, Ranganathan S, Subbana G N and Thangaraj N 1985 *Current Sci.* **54** 895
[14] Fung K K, Yang C Y, Zhou W Q, Zhao J G, Zhan W S and Shen B G 1986 *Phys. Rev. Lett.* **56** 2060
[15] Mackay A L 1982 *Physica* **114A** 66
[16] Kramer P and Neri R 1984 *Acta Crystallogr.* A **40** 580
[17] Audier M and Guyot P 1986 *Phil. Mag. Lett.* B **53** 43
[18] Elser V and Henley C 1985 *Phys. Rev. Lett.* **55** 2883
[19] Yamamoto A and Hiraga K 1988 *Phys. Rev.* B **37** 6207
[20] Cahn J W, Gratias D and Mozer B 1988 *J. Physique* **49** 1225
[21] Duneau M and Oguey C 1989 *J. Physique* **50** 135
[22] Guyot P and Audier M 1985 *Phil. Mag.* B **52** L15
[23] Henley C L and Elser V 1986 *Phil. Mag.* B **53** L59
[24] Fruchart R and Dubois J M 1987 *C. R. Acad. Sci., Paris* **305** 1413
[25] Janot C, de Boissieu M, Dubois J M and Pannetier J 1989 *J. Phys.: Condens. Matter* **1** 1029
[26] Knowles K M and Stobbs W M 1986 *Nature* **323** 312
[27] Knowles K M, Greer A L, Saxton W O and Stobbs W M 1985 *Phil. Mag.* B **52** L31
[28] Elser V 1985 *Phys. Rev.* B **32** 4892
[29] Hiraga K, Hirabayashi M, Inoue A and Masumoto T J 1985 *J. Phys. Soc. Japan* **54** 4077
[30] Dubois J M and Janot C 1987 *J. Physique* **48** 1981
[31] Hiraga K, Hirabayashi M, Inoue A and Masumoto T 1985 *Sci. Rep. Res. Inst. Tohoku Univ.* A **23** 309
[32] Kuriyama M, Long G G and Bendersky L 1985 *Phys. Rev. Lett.* **55** 849
[33] Dong C and Dubois J M 1992 *J. Non-Cryst. Solids* B submitted
[34] Duneau M and Katz A 1985 *Phys. Rev. Lett.* **54** 2688
[35] Kalugin P A, Kitaev A and Levitov L 1985 *J. Physique* **46** 1601
[36] Robinson K 1954 *Acta Crystallogr.* **7** 494
[37] Dong C, Dubois J M, de Boissieu M, Boudard M and Janot C 1991 *J. Materials Research* **6** 2637
[38] Pauling L 1960 *Nature of the Chemical Bond* 3rd edn (Ithaca, NY: Cornell University Press) p 425
[39] Mackay A L 1962 *Acta Crystallogr.* **15** 916
[40] Janot C, de Boissieu M, Dubois J M and Pannetier J 1989 *J. Phys.: Condens. Matter* **1** 1029
[41] Audier M, Sainfort P and Dubost B 1986 *Phil. Mag. Lett.* **54** L105
[42] de Boissieu M, Janot C, Dubois J M, Audier M and Dubost B 1991 *J. Phys.: Condens. Matter* **3** 1
[43] de Bruijn N G 1981 *Math. Proc.* A **84** 39
[44] Henley C L 1986 *Phys. Rev.* B **34** 797
[45] Levine O and Steinhardt P J 1986 *Phys. Rev.* B **34** 596
[46] Hiraga K, Hirabayashi M, Inoue A and Masumoto T 1987 *J. Microsc.* **146** 245
[47] Li F H and Liu W 1986 *Acta Crystallogr.* B **42** 336
[48] Shechtman D and Blech I A 1985 *Metall. Trans.* A **16** 1005
[49] van Tendeloo G, Van Landuyt J, Amelinckx S and Ranganathan S 1988 *J. Microsc.* **149** 1
[50] Audier M, Bréchet Y, de Boissieu M, Guyot P, Janot C and Dubois J M 1991 *Phil. Mag.* B **63** 1375
[51] Daulton T L, Kelton K F and Gibbons P C 1991 *Phil. Mag.* B **63** 687
[52] Lalla N P, Tiwari R S and Srivastava O N 1991 *Phil. Mag.* B **63** 629

[53] Kimura K, Hashimoto T, Suzuki K, Nagayama K, Ino H and Takeuchi S 1986 *J. Phys. Soc. Japan* **55-2** 534
[54] Dong C and Dubois J M 1991 *J. Mater. Sci.* **26** 1647
[55] Taylor M A 1959 *Acta Crystallogr.* **12** 393
[56] Yamamoto A and Ishihara K N 1988 *Acta Crystallogr.* A **44** 707
[57] Bancel P A, Heiney P A, Stephens P W, Goldman A I and Horn P M 1985 *Phys. Rev. Lett.* **54** 2422